Nonlinear IHS: A Promising Method for Pan-Sharpening

By

Morteza Ghahremani and Hassan Ghassemian

August 2016

Nonlinear IHS: A Promising Method for Pan-Sharpening

- **Published in:** IEEE Geoscience and Remote Sensing Letters
- **Volume:** 13
- **Issue:** 11
- **Page(s):** 1606-1610
- **Date of Publication:** 24 Aug. 2016
- **DOI:** 10.1109/LGRS.2016.2597271
- **Sponsored by:** IEEE Geoscience and Remote Sensing Society
- **Link(s):**

http://ieeexplore.ieee.org/document/7548323/

http://openremotesensing.net/index.php/codes/11-pansharpening/19-nonlinear-ihs-a-promising-method-for-pan-sharpening

Pan-Sharpening

- The goal of pan-sharpening is to increase the spatial resolution of the multi- or hyper-spectral images using a high spatial resolution panchromatic image.

- Pan-sharpening can be classified into four main categories:

1. component substitution-based methods such as [2]-[4], [16]-[20],
2. multiresolution analysis-based methods such as [5]-[8],
3. model-based methods such as [8]-[10], and
4. reconstruction-based methods such as [1],[8],[11],[12].

* Detailed surveys of pan-sharpening methods can be found in [13-15].

Local-Global Approach

- The goal of this letter is to introduce a Local-Global framework for pan-sharpening of multispectral images.

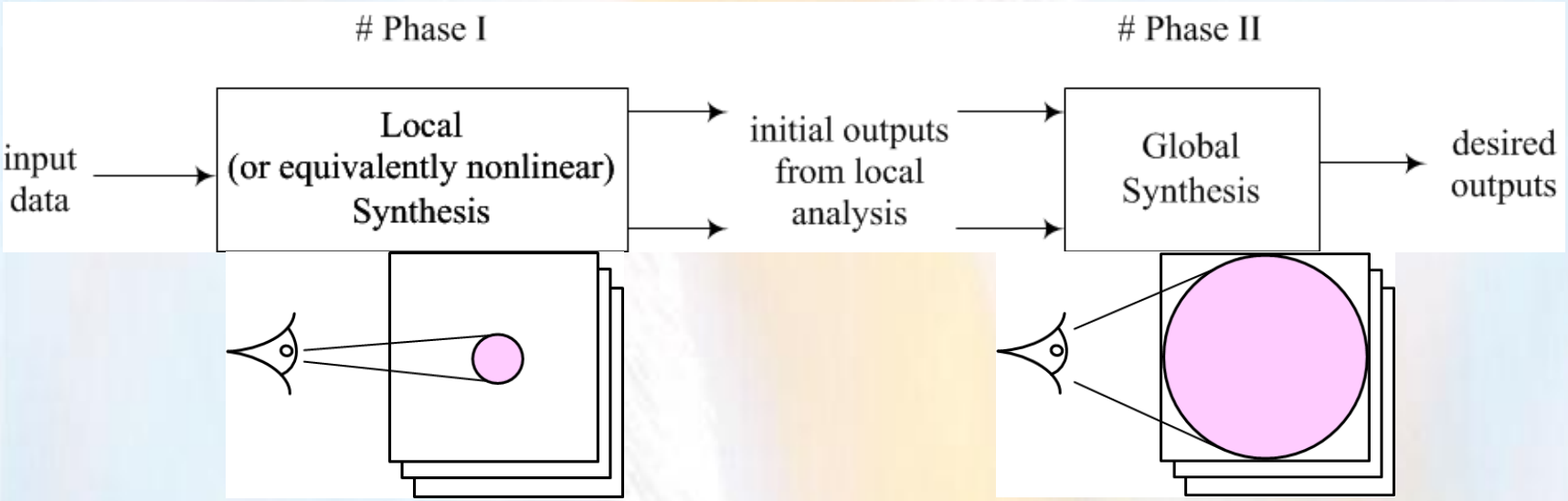

✓ The local-global framework is nothing but control your eyes!

Local-Global Approach

- The proposed approach can be implemented on any component-substitution methods.

- In this letter, we apply the proposed local-global approach to IHS.

Notation

- HRP: High-spatial Resolution Panchromatic
- LRP: Low-spatial Resolution Panchromatic
- LRM: Low-spatial Resolution Multispectral
- LRMup.: Upsampled Low-spatial Resolution Multispectral
- L: the number of spectral bands
- B: the size of a patch at low resolution ($B \in [3,5]$)
- ρ: the ratio of the spatial resolutions between the LRM and HRP images
- $\beta = \rho * B$ the size of a patch at high resolution
- q: the size of an overlapped region
- N: total number of patches in an image

INTENSITY-HUE-SATURATION (IHS)

- Tu *et al.* [2] expanded the original IHS and IHS-like methods and introduced a new framework for pan-sharpening:

$$M_{\mathrm{H}}^{k} = \mathrm{M}_{up.}^{k} + \left(\mathrm{P}_{his.} - I_{up.}\right), \qquad k = 1,\ldots,L$$

- M_{H} : the pan-sharpened images,
- M : the LRM images respectively,
- '*up.*' : the upsampling operator,
- $I_{up.}$: an upsampled intensity component which is obtained via

$$I_{up.} = \sum_{k=1}^{L} \omega_k y_{k,up.} = \boldsymbol{\omega}^{\mathrm{T}} \mathrm{M}_{up.};$$

INTENSITY-HUE-SATURATION (IHS)

- $P_{his.}$: histogram matched HRP data obtained through the following equation:

$$P_{his.} = \frac{\sigma_{I_{up.}}}{\sigma_P}(P - \mu_P) + \mu_{I_{up.}},$$

where ‘σ’ and ‘μ’ denote the standard deviation and mean.

- The main concern of IHS-based methods is how to accurately determine the weight vector.

- Authors in [16]-[18] assume a predetermined coefficients to estimate the intensity component and thus it generates spectral distortion.

INTENSITY-HUE-SATURATION (IHS)

- Rahmani et al. [19] proposed a modified IHS method defined as

$$M_{\mathrm{H}}^{k} = \mathrm{M}_{up.}^{k} + \mathbf{E}\left(\mathrm{P}_{his.} - I_{up.}\right), \qquad k = 1,\ldots,L.$$

Here, is $\mathbf{E}$ an edge detector which is equal to one on edges and equal to zero off edges

$$\mathbf{E} = exp(-\frac{\gamma}{\left|\nabla \mathrm{P}\right|^{4} + \varepsilon}),$$

- ∇ : the gradient operator
- γ : a parameter that controls the magnitude on the edges
- ε : a small value that enforces a nonzero denominator

INTENSITY-HUE-SATURATION (IHS)

- In the modified IHS method, the authors assume a non-negativity constraint on (2) to estimate the weight vector, i.e.

$$\hat{\boldsymbol{\omega}} = \arg\min_{\boldsymbol{\omega}} \left\| \mathrm{P}_{his.} - \boldsymbol{\omega}^{\mathrm{T}} \mathrm{M}_{up.} \right\|_2^2 + \lambda \left(\sum_{k=1}^{L} (\omega_k \geq 0) \right), \quad (6)$$

where $\boldsymbol{\omega} = (\omega_1, \ldots, \omega_L)^{\mathrm{T}}$ is the weight vector.

- The empirical results show the modified IHS method considerably improves the content of the pan-sharpened products.

The Main Drawbacks of Modified IHS Method

- The modified IHS method uses only the global synthesis approach to obtain the intensity component

drawback: it cannot deal with the local dissimilarities.

Thomas *et al.* [13] show that the global synthesis during pan-sharpening leads to significant spectral distortion because the structural patterns of the remote sensing data are complex.

- It is questionable whether the non-negativity constraint of the modified IHS method is reasonable.

drawback: This method cannot deal with redundancy.

The Main Drawbacks of Modified IHS Method

Redundancy is a common phenomenon which is often occurred in the spectral data due to the frequency overlaps of the spectral sensors. Thus, a non-negativity constraint cannot handle this common phenomenon.

- There is no specific trend to determine the Lagrangian parameter in (6).

drawback: this method uses s a predetermined Lagrangian parameter which cannot lead to the optimal weight vector.

The Main Characteristics of Proposed Nonlinear IHS Method

To overcome the modified IHS method's drawbacks, we introduce

- utilizing nonlinear synthesis (or local synthesis) approach instead of the common linear one to approximate the intensity component, and
- a global synthesis approach to make the intensity component at high spatial resolution consonant with its degraded one.
- Secondly, we use the energy constraint proposed in our previous research [1],[8] to overcome the second weakness of the modified IHS method.
- Thirdly, we propose a Singular Value Decomposition (SVD) approach to seek the best Lagrangian parameter that leads to the optimal weight vector.

The Main Characteristics of Proposed Nonlinear IHS Method

- Finally, we use both the original and upsampled LRM data as well as both the HRP data and its degraded version during the weight vector estimation. This procedure makes the weight vector results stable.

IHS Via a Local-Global Approach

- The goal is to estimate intensity component via a local-global framework

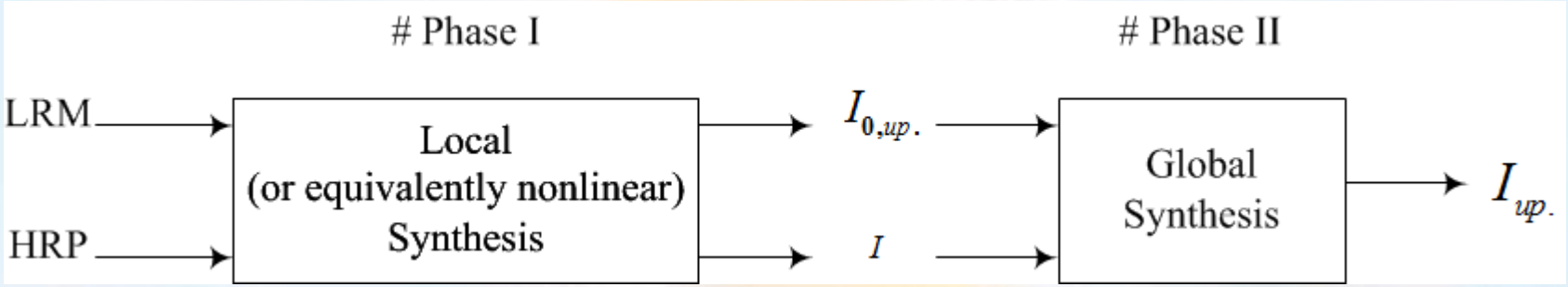

Phase I: Nonlinear(local) synthesis

- The goal of this stage is to estimate the intensity component and an initial upsampled intensity component.

- In order to estimate the optimum intensity component, we use a patch-by-patch strategy.

Additional Notations

- $\mathrm{X}^{(i)} = (\mathrm{X}_{1,1}, \ldots, \mathrm{X}_{1,\beta}, \ldots, \mathrm{X}_{\beta,1}, \ldots, \mathrm{X}_{\beta,\beta})^{\mathrm{T}}$: the *i*-patch of the HRP image
- $\mathrm{x}^{(i)} = (\mathrm{x}_{1,1}, \ldots, \mathrm{x}_{1,B}, \ldots, \mathrm{x}_{B,1}, \ldots, \mathrm{x}_{B,B})^{\mathrm{T}}$: the *i*-patch of the LRP image

- $S^{(i)} = (S_{1,1}, \ldots, S_{1,\beta}, \ldots, S_{\beta,1}, \ldots, S_{\beta,\beta})^{\mathrm{T}}$: the *i*-patch of the upsampled intensity component
- $s^{(i)} = (s_{1,1}, \ldots, s_{1,B}, \ldots, s_{B,1}, \ldots, s_{B,B})^{\mathrm{T}}$: the *i*-patch of the intensity component

- $\mathrm{Y}^{(i)} = (y_1^{(i)}, \ldots, y_k^{(i)})^{\mathrm{T}}$: the *i*-patch of the entire original LRM bands
- $\mathrm{Y}_{up.}^{(i)} = (y_{1,up.}^{(i)}, \ldots, y_{k,up.}^{(i)})^{\mathrm{T}}$: the *i*-patch of the entire upsampled LRM bands

Phase I: Nonlinear(local) synthesis

- The intensity component can be approximated as a linear or nonlinear combination of the spectral bands.
- As the structural characteristics of the remote sensing satellites data are more complex than the natural data, we apply a nonlinear model.
- A nonlinear model can relax the linear one in most of remote sensing applications.
- To implement the nonlinear model, a possible solution is to partition the data into small subimages / patches and then to apply the linear model on each patch.

Phase I: Nonlinear(local) synthesis

- Be vigilant! when tiling an image into patches, a windowing effect is occurred.
- The windowing effect can be resolved by the overlapping approach.
- We apply the smooth window presented in [§] instead of the conventional averaging approach in the overlapped regions. This issue will be discussed in more detail.

[§] A compressed-sensing-based pan-Sharpening method for spectral distortion reduction. *IEEE Trans. Geosci. Remote Sens.*, vol. 54, no. 4, pp. 2194–2206, Apr. 2016.

Phase I: Nonlinear(local) synthesis

- For each patch , we apply the linear model on the LRM patches to form the intensity component patches, i.e.,

$$s^{(i)} = \sum_{k=1}^{L} \omega_k^{(i)} y_k^{(i)} = \boldsymbol{\omega}^{(i),\mathrm{T}} \mathrm{Y}^{(i)},$$

&

$$S^{(i)} = \sum_{k=1}^{L} \omega_k^{(i)} y_{k,up.}^{(i)} = \boldsymbol{\omega}^{(i),\mathrm{T}} \mathrm{Y}_{up.}^{(i)}.$$

Phase I: Nonlinear(local) synthesis

- To minimize the spectral distortion, the intensity component should approximate the HRP data as closely as possible, i.e.,

$$\hat{\boldsymbol{\omega}}^{(i)} = \arg\min_{\boldsymbol{\omega}^{(i)}} \left\{ \left\| \tilde{\mathrm{X}}^{(i)} - \boldsymbol{\omega}^{(i),\mathrm{T}} \tilde{\mathrm{Y}}^{(i)} \right\|_2^2 \right\} \quad \text{s.t.} \quad \boldsymbol{\omega}^{(i),\mathrm{T}} \boldsymbol{\omega}^{(i)} = 1, \qquad (*)$$

where

$$\tilde{\mathrm{X}}^{(i)} = \begin{bmatrix} \mathrm{X}^{(i)} \\ \mathrm{x}^{(i)} \end{bmatrix}, \qquad \tilde{\mathrm{Y}}^{(i)} = \begin{bmatrix} \mathrm{Y}_{up.}^{(i)} \\ \mathrm{Y}^{(i)} \end{bmatrix}.$$

- ✓ In (*), the energy constraint term determines the energy level of each spectral band involved in the intensity component approximation. This constraint is favorable to overcome the redundancy of the remote sensing data and to better investigate the local dissimilarities [1], [8].
- ✓ we stack the input data to have a stable weight vector.

Solution of (9)

- Lagrangian multiplier offers an equivalent formulation to (*)

$$\Omega\left(\boldsymbol{\omega}^{(i)},\lambda^{(i)}\right)=\left\|\tilde{\mathrm{X}}^{(i)}-\boldsymbol{\omega}^{(i),\mathrm{T}}\tilde{\mathrm{Y}}^{(i)}\right\|_2^2+\lambda^{(i)}\left(\boldsymbol{\omega}^{(i),\mathrm{T}}\boldsymbol{\omega}^{(i)}-1\right),\quad (+)$$

where $\lambda\geq 0$ is a Lagrangian multiplier that plays the role of the a dual variable.

- Minimizing $\Omega(\boldsymbol{\omega}^{(i)},\lambda^{(i)})$ over $\boldsymbol{\omega}^{(i)}$, we can obtain the Lagrangian dual:

$$\Gamma(\lambda^{(i)})=\arg\min_{W^{(i)}}\ \Omega(\boldsymbol{\omega}^{(i)},\lambda^{(i)})=\tilde{\mathrm{X}}^{(i),\mathrm{T}}\tilde{\mathrm{X}}^{(i)}-$$

$$(\tilde{\mathrm{Y}}^{(i),\mathrm{T}}\tilde{\mathrm{X}}^{(i)})^{\mathrm{T}}(\tilde{\mathrm{Y}}^{(i),\mathrm{T}}\tilde{\mathrm{Y}}^{(i)}+\lambda^{(i)}\mathbf{I})^{-1}\tilde{\mathrm{Y}}^{(i),\mathrm{T}}\tilde{\mathrm{X}}^{(i)},\quad (\times)$$

where ‘ $\mathbf{I}$ ’ is an identity matrix of size ‘L’.

Solution of (9)

- The gradient of for the patch can be computed as follows:

$$\frac{\mathrm{d}}{\mathrm{d}\lambda^{(i)}}\Gamma(\lambda^{(i)}) = \left\|\tilde{\mathrm{X}}^{(i),\mathrm{T}}\tilde{\mathrm{Y}}^{(i)}(\tilde{\mathrm{Y}}^{(i),\mathrm{T}}\tilde{\mathrm{Y}}^{(i)} + \lambda^{(i)}\mathbf{I})^{-1}\right\|_2^2 - 1.$$

&

$$\frac{\mathrm{d}^2}{\mathrm{d}\lambda^{(i),2}}\Gamma(\lambda^{(i)}) = -2\tilde{\mathrm{Y}}^{(i),\mathrm{T}}\tilde{\mathrm{X}}^{(i)}\left(\tilde{\mathrm{Y}}^{(i),\mathrm{T}}\tilde{\mathrm{Y}}^{(i)} + \lambda^{(i)}\mathbf{I}\right)^{-1}$$

$$\left\{\left(\tilde{\mathrm{Y}}^{(i),\mathrm{T}}\tilde{\mathrm{Y}}^{(i)} + \lambda^{(i)}\mathbf{I}\right)^{-1}\left(\tilde{\mathrm{Y}}^{(i),\mathrm{T}}\tilde{\mathrm{X}}^{(i)}\right)\right.$$

$$\left.\left(\tilde{\mathrm{Y}}^{(i),\mathrm{T}}\tilde{\mathrm{X}}^{(i)}\right)^{\mathrm{T}}\left(\tilde{\mathrm{Y}}^{(i),\mathrm{T}}\tilde{\mathrm{Y}}^{(i)} + \lambda^{(i)}\mathbf{I}\right)^{-1}\right\}.$$

Solution of (9)

- Now, we optimize the Lagrange dual using Newton's method. After maximizing, we obtain the optimal the weight vector as follows:

$$\hat{\boldsymbol{\omega}}^{(i)} = \left(\tilde{\mathrm{Y}}^{(i),\mathrm{T}} \tilde{\mathrm{Y}}^{(i)} + \hat{\lambda}^{(i)} \mathbf{I} \right)^{-1} \tilde{\mathrm{Y}}^{(i),\mathrm{T}} \tilde{\mathrm{X}}^{(i)}, \qquad \forall i = 1,...,N. \quad (\#)$$

- A fast implementation of the weight vector estimator can be done through SVD approach [21].

Algorithm: Approximate the Solution of (9)

- **For** each patch i, $i \in \{1, \ldots, N\}$

Compute $\mathrm{SVD}(\tilde{\mathrm{Y}}^{(i)}) = U^{(i)}\Sigma^{(i)}V^{(i),\mathrm{T}} = \sum_{j=1}^{L} \sigma_j^{(i)} u_j^{(i)} v_j^{(i),\mathrm{T}}$

- if $\sum_{j=1}^{L} \left(\frac{u_j^{(i)} \tilde{\mathrm{X}}^{(i)}}{\sigma_j^{(i)}} \right)^2 = 1$, then $\hat{\boldsymbol{\omega}}^{(i)} = \sum_{j=1}^{L} \left(\frac{u_j^{(i)} \tilde{\mathrm{X}}^{(i)}}{\sigma_j^{(i)}} \right) v_j^{(i)}$.

else

Apply Newton's method to find $\lambda_+^{(i)}$ such that $\sum_{j=1}^{L} \left(\frac{\sigma_j^{(i)} u_j^{(i)} \tilde{\mathrm{X}}^{(i)}}{\sigma_j^{(i),2} + \lambda_+^{(i)}} \right)^2 = 1$.

$$\hat{\boldsymbol{\omega}}^{(i)} = \sum_{j=1}^{L} \left(\frac{\sigma_j^{(i)} u_j^{(i)} \tilde{\mathrm{X}}^{(i)}}{\sigma_j^{(i),2} + \lambda_+^{(i)}} \right) v^{(i)}$$

end

* **code:** Fast_Energy_based_W_Estimator.m

Smooth Window vs. Averaging Method!

- Which strategy can we apply in an overlapped region? smooth window or averaging method?

- Averaging method:

In an overlapped region, this method calculates the average of two overlapped patches pixel-by-pixel.

Smooth Window

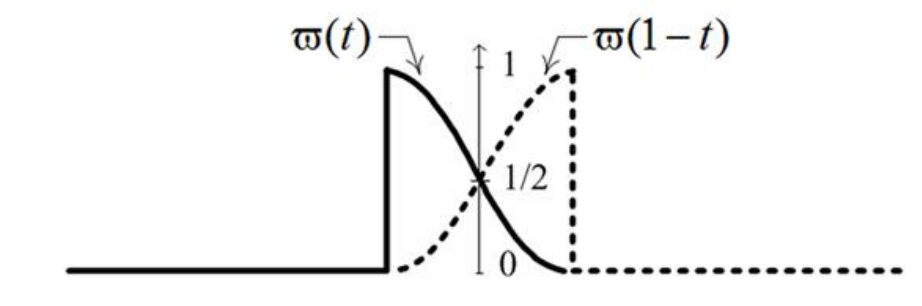

- a smooth window should

  1- satisfy $\varpi(0)=1$ and $\varpi(1)=0$,

  2- obey the symmetry property: $\varpi(t)+\varpi(1-t)=1$

Example: $\varpi(t)=cos^2(\pi t/P)$

* code: CosineWindow.m

Calculation of a Smooth Window in Vertically Overlapping of Size [*P q*]

- Y: an HRM image patch
- Code: Overlapping.m
- For the *i*- and (*i*+1)-th patches

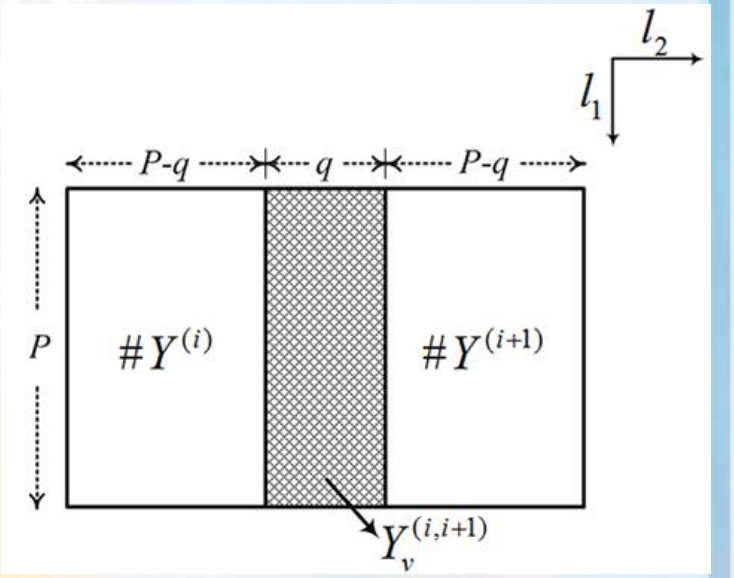

$$Y_{v,(k)}^{(i,i+1)}(l_1,l_2) = \varpi(l_2)\, Y^{(i)}(l_1,l_2) + \varpi(q-1-l_2)\, Y^{(i+1)}(l_1,q-1-l_2),$$

$$l_1 = 0,\ldots,P-1 \;\&\; l_2 = 0,\ldots,q-1 \;\&\; k \in \{1,\ldots,L\},$$

Calculation of a Smooth Window in Horizontally Overlapping of Size [*q P*]

- For the j- and $(j+1)$-th patches

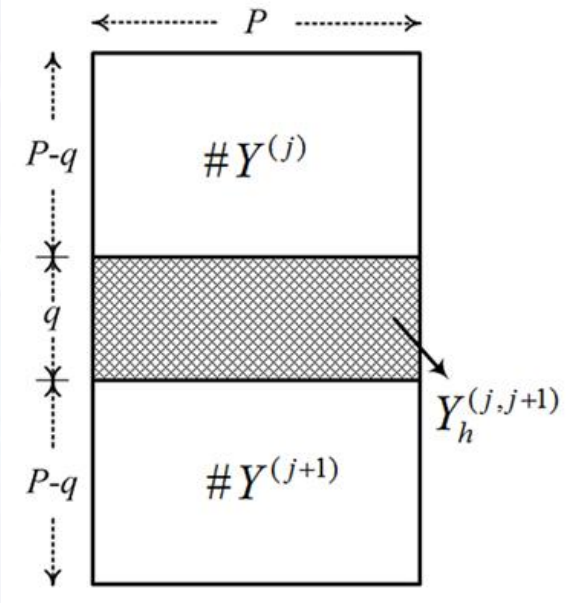

$$Y_{h,(k)}^{(j,j+1)}(l_1,l_2) = \varpi(l_1)\, Y^{(j)}(l_1,l_2) + \varpi(q-1-l_1)\, Y^{(j+1)}(q-1-l_1,l_2),$$

$$l_1 = 0,\ldots,q-1 \;\&\; l_2 = 0,\ldots,P-1 \;\&\; k \in \{1,\ldots,L\}.$$

Experimental Results with Smooth Window vs. Averaging Method

- Deimos data:
  - P = 8, q=5 (at high resolution)
  - Code: Demo_Overlapping.m

Methods	CC $(I_{up.}, \text{HRP})$	Norm1 $(I_{up.}, \text{HRP})$
Reference Value	1	0
Averaging Method	0.769	110.39
Smooth Window	0.783	106.77

Experimental Results

- WorldView-2:
  - ✓ The size of images: 512×512
  - ✓ HRP : 1.84 m
  - ✓ LRM : 7.36 m
  - ✓ $L = 8$
  - ✓ $\rho = 4$
  - ✓ RGB: bands 5, 3, and 2

Phase II: Global Synthesis

- The intensity components obtained through the local synthesis approach (I and $I_{0,up.}$) may not satisfy the global reconstruction - $I = \mathbf{M}I_{up.}$ - exactly ($\mathbf{M}$ is a downscaling operator)
- Thus we have

$$\hat{I}_{up.} = \arg\min_{I_{up.}} \left\| I - \mathbf{M}I_{up.} \right\|_2^2 + \eta \left\| I_{up.} - I_{0,up.} \right\|_2^2$$

η : this parameter tries to keep a balance between the reconstruction constraint fidelity and the initial estimated intensity component given by the local synthesis approach.

Phase II: Global Synthesis

- Gradient descent is a possible solution to this optimization problem:

$$I_{up.}^{t+1} = I_{up.}^{t} + \upsilon\left[\mathbf{M}^{\mathrm{T}}\left(I - \mathbf{M}I_{up.}^{t}\right) + \eta\left(I_{up.}^{t} - I_{0,up.}\right)\right],$$

υ : the step size of the gradient descent

$I_{up.}^{t}$: the estimation of $I_{up.}$ after 't' iteration

Experimental Results with Global Synthesis

- Deimos data:
  - t = 10 (number of iterations), $\upsilon = t$ ^-1(i.e., 0.1)
  - code: Demo_GlobalSynthesis.m

Methods	CC $\left(I_{up.,degraded}, I\right)$	Norm1 $\left(I_{up.,degraded}, I\right)$
Reference Value	1	0
Without Global Synthesis	0.954	4.172
Global Synthesis	0.9983	0.692

Experimental Results with Deimos data

- Deimos data:
  - ✓ code: Demo_NonlnearIHS.m
  - ✓ The size of data: 512×512 pixels
  - ✓ HRP : 1 m
  - ✓ LRM : 4 m
  - ✓ $L = 4$
  - ✓ $\rho = 4$
  - ✓ RGB: bands 2, 3, and 4

Reference LRM

Generalized IHS

Modified IHS

Nonlinear IHS

The Performance of Fusion Results with Deimos data

Methods	CC (Avg.)	RMSE (Avg.)	Q (Avg.)	SAM (deg.)	QNR		
					D_s	D_λ	Avg.
Reference Value	1	0	0	0	0	0	1
Generalized IHS	0.658	18.66	0.837	14.65	0.318	0.170	0.567
Modified IHS	0.782	10.63	0.875	10.06	0.253	0.103	0.670
Nonlinear IHS	0.948	04.84	0.967	03.64	0.130	0.045	0.831

The Performance of IHS-Based Methods in Estimating the Intensity Component

Methods	CC $(I_{up.}, \text{HRP})$	CC (I, LRP)	RMSE $(I_{up.}, \text{HRP})$	RMSE (I, LRP)
Reference Value	1	1	0	0
Generalized IHS	0.632	0.773	22.21	7.443
Modified IHS	0.696	0.835	14.66	5.650
Nonlinear IHS	0.865	0.911	09.33	2.201

Dependence on Patch Size and Overlapping Area Size

Patch Size	Overlapped pixels	CC (Avg.)	RMSE (Avg.)
3	1	0.955	3.51
4	1	0.948	3.85
4	2	0.975	2.42
5	1	0.928	4.65
5	2	0.948	3.19
5	3	0.965	2.83

Experimental Results with WorldView-2 data

- WorldView-2 data:
  - ✓ The size of data: 512×512 pixels
  - ✓ HRP : 1.84 m
  - ✓ LRM : 7.36 m
  - ✓ $L = 8$
  - ✓ $\rho = 4$
  - ✓ RGB: bands 5, 3, and 2

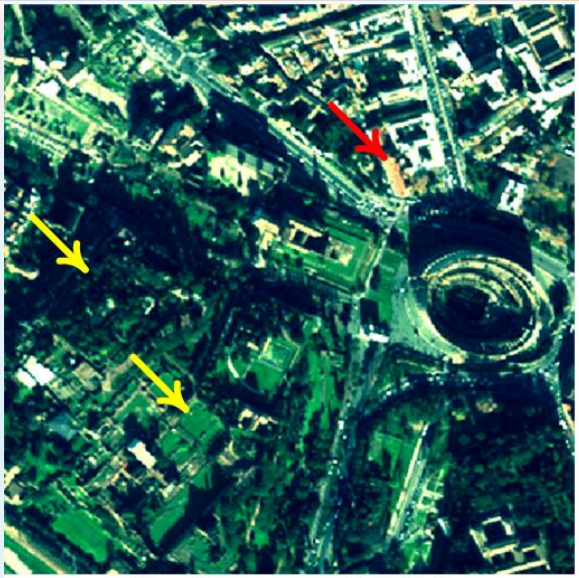

Reference LRM

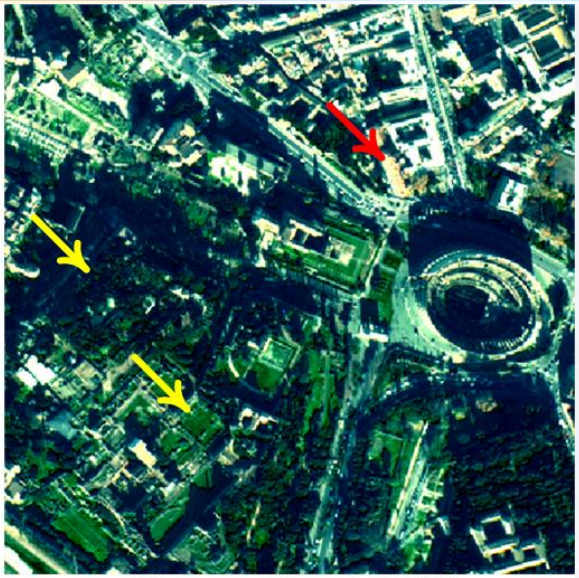

Generalized IHS

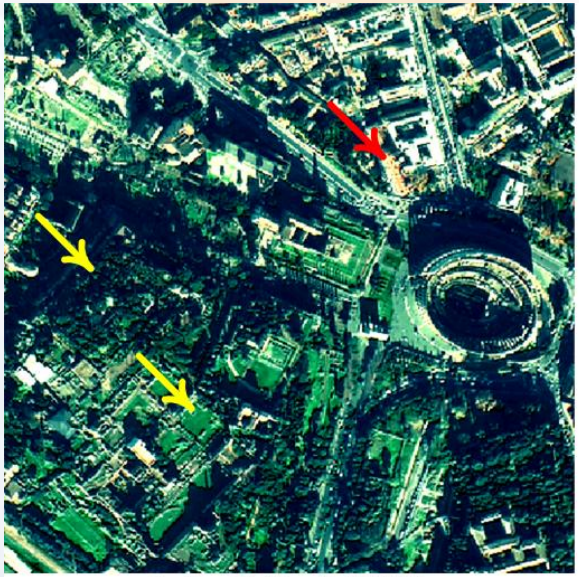

Modified IHS

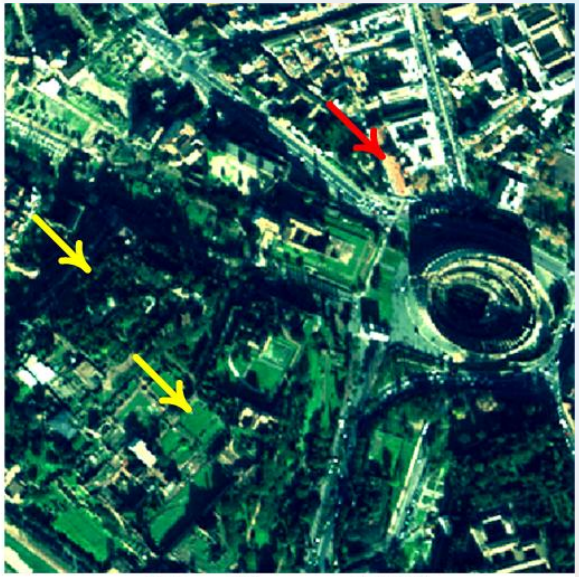

Nonlinear IHS

The Performance of Fusion Results with WorldView-2 data

Methods	CC (Avg.)	RMSE (Avg.)	Q (Avg.)	SAM (deg.)	QNR		
					D_s	D_λ	Avg.
Reference Value	1	0	0	0	0	0	1
Generalized IHS	0.753	14.27	0.684	11.30	0.332	0.153	0.566
Modified IHS	0.839	11.40	0.703	08.85	0.324	0.107	0.603
Nonlinear IHS	0.968	03.27	0.751	02.14	0.218	0.027	0.761

Time Costs (sec.) of the Different Pan-Sharpening Methods for the 512×512 Data CPU Core i7 and RAM 6 GB

- ✓ CPU = Core i7, 2.2 GHz
- ✓ RAM = 6 GB

Methods	DEIMOS-2	WorldView-2
Generalized IHS	0.05	0.07
Modified IHS	0.39	0.4
Nonlinear IHS	2.55	2.6

Question ?

- The patch size B is chosen between 3 and 5. However, in [1] or [8], which are compressive sensing-based methods, the authors suggest the patch size B is typically varying from 4 to 8. Are there some relationships between best patch size and spatial resolutions of LRM?

Answer: To better illustrate how to determine the patch size, we first explain the procedure of determining the patch size in [1] or [8].

- In [1] or [8], we use compressive sensing theory to recovery the intensity component.
- According to this theory, we can recover an unknown sparse signal / patch from a small set of linear projections; ‘set of signals’ is called dictionary. According to this theory, we have two sets of signal or equivalently dictionaries:

- LSD = low scale dictionary: this dictionary contains an arbitrary number of lower scale signals of size ‘B’.
- HSD = high scale dictionary: this dictionary contains higher scale signals of size ‘ρ*B’, in which each higher scale signal in HSD is corresponding to the lower scale one in LSD.

The key point of compressive sensing theory is to sparsely represent a signal at lower scale in LSD, and then to expand the same relationships onto HSD to obtain the higher scale signal.

✓ Thus, in this case there is a close relationship between the patch sizes at lower and higher scales. In other words, we should choose ‘B’ that yields to sparser image. A too small image patch size renders LSD not to be compact, i.e., the atoms in LSD is generally highly coherent. On the other hand, a too large image patch size endangers the sparse representation of the higher scale patches in the dictionary, i.e., the atoms in the dictionary should contain primitive patterns instead of specific objects (according to this theory, ‘B=2’ or ‘B=3’ maybe endangers the sparsity of signal at lower scale).

- ✓ Moreover, this theory depends on overlapping area size. We would like to have a dictionary with atoms of compact support and minimal overlap (to minimize the coherence among the atoms). There is also a tradeoff between completeness and compactness of the dictionary. Finally, in [1, 8] we assess the results for different 'B' (B varies from 4 to 8) and then the best 'B' is chosen based on the fidelity between proper quantitative results and running time.

- However, in NIHS the issue of patch size is completely different from [1, 8]. In this paper, there is no concern about sparsity and we can choose lower patch sizes. For instance, we are sure that that the 63th patch of the upsampled intensity component is exactly obtained through the 63th patches of upsampled LRM and HRP data.

- So we do not seek other patches from a dictionary as we do in the compressive sensing-based methods. In other words, the aim of the current paper is to decrease the nonlinearity of the data. A possible solution is to partition the data into small patches and then to apply the linear model on each patch (see the following figure).

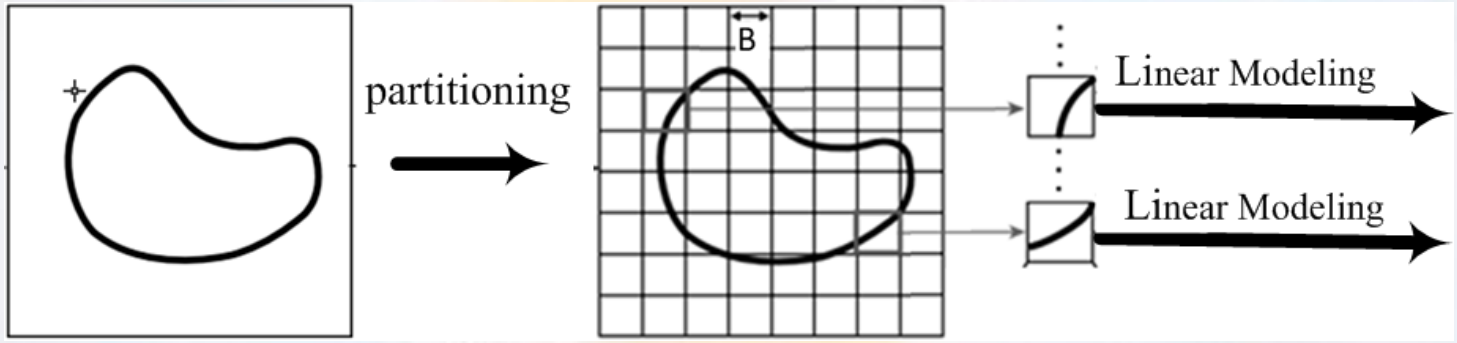

The procedure of linear representation of a nonlinear image

- Thus, decreasing the patch size ‘B’ results in increase in linearity, but it also makes high computation time. Practically 3<=B<=5 yields satisfactory results. Moreover, overlapping size is typically chosen between 1 and [B/2].

Thank you

If you have any questions, please do not hesitate to contact me by

morteza.ghahremani.b@gmail.com

morteza.ghahremani@modares.ac.ir

The authors would like to thank Professor Jocelyn Chanussot for sharing our code and paper.

References

[1] M. Ghahremani and H. Ghassemian, "A compressed-sensing-based pan-Sharpening method for spectral distortion reduction," *IEEE Trans. Geosci. Remote Sens.*, vol. 54, no. 4, pp. 2194–2206, Apr. 2016.

[2] T.M. Tu, S.C. Su, H.C. Shyu, and P. S. Huang, "A new look at IHS like image fusion methods," *Inf. Fusion*, vol. 2, no. 3, pp. 177–186, Sep. 2001.

[3] C. A. Laben and B. V. Brower, "Process for enhancing the spatial resolution of multispectral imagery using pan-sharpening," U.S. Patent 6011875, Jan. 4, 2000.

[4] P. S. Chavez, S. C. Sides, and J. A. Anderson, "Comparison of three different methods to merge multiresolution and multispectral data Landsat TM and SPOT panchromatic," *Photogramm. Eng. Remote Sens.*, vol. 57, no. 3, pp. 295–303, Mar. 1991.

[5] J. Nunez, X. Otazu, O. Fors, A. Prades, V. Pala, and R. Arbiol, "Multiresolution-based image fusion with additive wavelet decomposition," *IEEE Trans. Geosci. Remote Sens.*, vol. 37, no. 3, pp. 1204–1211, May 1999.

[6] M. Ghahremani and H. Ghassemian, "Remote sensing image fusion based on curvelets and ICA," *Int. J. Remote Sens.*, vol. 36, no. 16, pp. 4131–4143, Aug. 2015.

[7] M. Choi, R. Y. Kim, M. R. Nam, and H. O. Kim, "Fusion of multispectral and panchromatic satellite images using the curvelet transform," *IEEE Geosci. Remote Sens. Lett.*, vol. 2, no. 2, pp. 136–140, Apr. 2005.

[8] M. Ghahremani and H. Ghassemian, "Remote sensing image fusion using ripplet transform and compressed sensing," *IEEE Geosci. Remote Sens. Lett.*, vol. 12, no. 3, pp. 502–506, Mar. 2015.

[9] L. Zhang, H. Shen, W. Gong, and H. Zhang, "Adjustable model-based fusion method for multispectral and panchromatic images," *IEEE Trans. Syst., Man, Cybern. B, Cybern.*, vol. 42, no. 6, pp. 1693–1704, Dec. 2012.

[10] M. V. Joshi, L. Bruzzone, and S. Chaudhuri, "A model-based approach to multiresolution fusion remotely sensed images," *IEEE Trans. Geosci. Remote Sens.*, vol. 44, no. 9, pp. 2549–2562, Sep. 2006.

[11] S. Li and B. Yang, "A new pan-sharpening method using a compressed sensing technique," *IEEE Trans. Geosci. Remote Sens.*, vol. 49, no. 2, pp. 738–746, Feb. 2011.

[12] C. Jiang, H. Zhang, H. Shen, and L. Zhang, "Two-step sparse coding for the pan-sharpening of remote sensing images," *IEEE J. Sel. Topics Appl. Earth Observ. Remote Sens.*, vol. 7, no. 5, pp. 1792–1805, May 2014.

[13] C. Thomas, T. Ranchin, L. Wald, and J. Chanussot, "Synthesis of multispectral images to high spatial resolution: A critical review of fusion methods based on remote sensing physics," *IEEE Trans. Geosci. Remote. Sens.*, vol. 46, no. 5, pp. 1301–1312, May 2008.

[14] L. Gomez-Chova, D. Tuia, G. Moser, and G. Camps-Valls, "Multimodal classification of remote sensing images: A review and future directions," *Proc. IEEE*, vol. 103, no. 9, pp. 1560–1584, Sep. 2015.

[15] H. Ghassemian, "A review of remote sensing image fusion methods," *Inf. Fusion*, vol. 32, no. 9, pp. 75–89, Nov. 2016.

[16] T. M. Tu, P. S. Huang, C. L. Hung, and C. P. Chang, “A fast intensity-hue-saturation fusion technique with spectral adjustment for IKONOS imagery,” *IEEE Geosci. Remote Sens. Lett.*, vol. 1, no. 4, pp. 309–312, Oct. 2004.

[17] M. Choi, “A new intensity-hue-saturation fusion approach to image fusion with a tradeoff parameter,” *IEEE Trans. Geosci. Remote Sens.*, vol. 44, no. 6, pp. 1672–1682, Jun. 2006.

[18] M. C. El-Mezouar, N. Taleb, K. Kpalma, and J. Ronsin, “An IHS-based fusion for color distortion reduction and vegetation enhancement in IKONOS imagery,” *IEEE Trans. Geosci. Remote Sens.*, vol. 49, no. 5, pp. 1590–1602, May 2011.

[19] S. Rahmani, M. Strait, D. Merkurjev, M. Moeller, and T. Wittman, “An adaptive IHS pan-sharpening method,” *IEEE Geosci. Remote Sens. Lett.*, vol. 7, no. 4, pp. 746–750, Oct. 2010.

[20] Y. Leung, J. Liu, and J. Zhang, “An improved adaptive intensity–hue–saturation method for the fusion of remote sensing images,” *IEEE Geosci. Remote Sens. Lett.*, vol. 11, no. 5, pp. 985–989, May 2014.

[21] G. H. Golub and C. F. Van Loan, *Matrix Computations*. The Johns Hopkins Univ. Press, 2013, pp. 313–317.

[22] T. Ranchin and L. Wald, “Fusion of high spatial and spectral resolution images: The ARSIS concept and its implementation,” *Photogramm. Eng. Remote Sens.*, vol. 66, no. 1, pp. 49–61, Jan. 2000.

[23] L. Alparone, B. Aiazzi, S. Baronti, A. Garzelli, and P. Nencini, “A global quality measurement of pan-sharpened multispectral imagery,” *IEEE Geosci. Remote Sens. Lett.*, vol. 1, no. 4, pp. 313–317, Oct. 2004.

[24] R. H. Yuhas, A. F. H. Goetz, and J.W. Boardman, “Discrimination among semi-arid landscape endmembers using the Spectral Angle Mapper (SAM) algorithm,” in *Proc. Summaries 3rd Annu. JPL Airborne Geosci. Workshop*, 1992, pp. 147–149.

[25] L. Alparone, B. Aiazzi, S. Baronti, A. Garzelli, F. Nencini, and M. Selva, “Multispectral and panchromatic data fusion assessment without reference,” *Photogramm. Eng. Remote Sens.*, vol. 74, no. 2, pp. 193–200, Feb. 2008.